

A full quantal theory of one-neutron halo breakup reactions

R. Chatterjee*

Theory Group, Saha Institute of Nuclear Physics,

1/AF, Bidhannagar, Kolkata 700064, India.

(Dated: November 19, 2018)

We present a theory of one-neutron halo breakup reactions within the framework of post-form distorted wave Born approximation wherein pure Coulomb, pure nuclear and their interference terms are treated consistently in a single setup. This formalism is used to study the breakup of one-neutron halo nucleus ^{11}Be on several targets of different masses. We investigate the role played by the pure Coulomb, pure nuclear and the Coulomb-nuclear interference terms by calculating several reaction observables. The Coulomb-nuclear interference terms are found to be important for more exclusive observables.

PACS numbers: 25.60.-t, 25.60.Gc, 24.10.Eq, 24.50.+g

Keywords: halo nuclei, Coulomb breakup, nuclear breakup, Coulomb-nuclear interference.

I. INTRODUCTION

Our current understanding of most of the processes governing the nuclear systems is based on studies made with stable nuclei, which constitute less than ten percent of all the nuclei known to exist in nature. Away from the valley of stability there are a large number of nuclei having very short half lives and very small one- and two-nucleon separation energies. Many of them exhibit a halo structure in their ground states in which loosely bound valence nucleon(s) has (have) a large spatial extension with respect to the respective core [1, 2, 3, 4]. We still lack a fully microscopic understanding of the stability of these unique many body systems.

These nuclei are also important from nuclear astrophysics point of view. The r-process and the s-process paths which together are dominant mechanisms for nucleosynthesis of

*Electronic address: raja@theory.saha.ernet.in

heavy elements above iron, pass through the region of neutron rich exotic nuclei, in the Segré chart. Properties of these nuclei are, therefore, important inputs to theoretical calculations of stellar burning which otherwise are often forced to rely on global assumptions about nuclear masses, decays and level structures extracted from stable nuclei.

Projectile breakup reactions have played a major role in unraveling the structure and properties of halo nuclei. However it is clear that pure Coulomb [5, 6, 7, 8, 9, 10, 11] or pure nuclear [12, 13, 14] breakup calculations may not be fully sufficient to describe all the details of the halo breakup data which have been increasing rapidly both in quality and quantity [15, 16, 17, 18, 19]. In majority of them both Coulomb and nuclear breakup effects as well as their interference terms are likely to be significant and the neglect of the latter terms may not be justified [20, 21, 22, 23]. A theory which can take care of the Coulomb and nuclear breakup effects as well as their interference terms on an equal footing is an important requirement in interpreting the data obtained from the experiments done already or are planned to be done in future.

For breakup reactions of light stable nuclei, such a theory has been developed [24] within the framework of post-form distorted wave Born approximation (DWBA), which successfully describes the corresponding data at low beam energies. However, since it uses the simplifying approximation of a zero-range interaction [25] between constituents of the projectile, it is inapplicable to cases where the internal orbital angular momentum of the projectile is different from zero.

Recently, we have presented a theory [26, 27] to describe the breakup reactions of one-nucleon halo nuclei within the post-form DWBA (PFDWBA) framework, that consistently includes both Coulomb and nuclear interactions between the projectile fragments and the targets to all orders, but treats the fragment-fragment interaction in first order. The Coulomb and nuclear breakups along with their interference term are treated within a single setup in this theory. The breakup contributions from the entire continuum corresponding to all the multipoles and the relative orbital angular momenta between the valence nucleon and the core fragment are included in this theory where finite range effects are treated by a local momentum approximation (LMA) [28, 29]. Full ground state wavefunction of the projectile, of any angular momentum structure, enters as an input to this theory.

The Coulomb-nuclear interference (CNI) terms have also been calculated using the prior-form DWBA [30] and within models [31, 32] where the time evolution of the projectile in

coordinate space is described by solving the time dependent Schrödinger equation, treating the projectile-target (both Coulomb and nuclear) interaction as a time dependent external perturbation. Recently, within an eikonal-like framework, Coulomb and nuclear processes have also been treated within the same framework in Ref. [33].

In this paper, we present more details of the formalism of PFDWBA breakup theory and of its application to breakup reactions of the one-neutron halo nucleus ^{11}Be on targets of masses spanning a wide range in the periodic table. We investigate the role played by the pure Coulomb, pure nuclear and the CNI terms by calculating different breakup observables. Our formalism is presented in section II. In section III, we present and discuss the results of our calculations for various observables for the breakup of ^{11}Be on various targets. Summary and conclusions of our work are presented in section IV. Additional discussions on the validity of the LMA relevant for our case are presented in Appendix A.

II. FORMALISM

We consider the elastic breakup reaction, $a + t \rightarrow b + c + t$, in which the projectile a ($a = b + c$) breaks up into fragments b and c (both of which can be charged) in the Coulomb and nuclear fields of a target t . The triple differential cross section for this reaction is given by

$$\frac{d^3\sigma}{dE_b d\Omega_b d\Omega_c} = \frac{2\pi}{\hbar v_a} \rho(E_b, \Omega_b, \Omega_c) \sum_{\ell m} |\beta_{\ell m}|^2, \quad (1)$$

where v_a is the relative velocity of the projectile with respect to the target, ℓ is the orbital angular momentum for the relative motion of b and c in the ground state of a , and $\rho(E_b, \Omega_b, \Omega_c)$ is the appropriate phase space factor (see, e.g., Ref. [9]). The reduced transition amplitude, in Eq. (1), $\beta_{\ell m}$ is defined as

$$\begin{aligned} \hat{\ell}\beta_{\ell m}(\mathbf{k}_b, \mathbf{k}_c; \mathbf{k}_a) = & \int d\mathbf{r}_1 d\mathbf{r}_i \chi_b^{(-)*}(\mathbf{k}_b, \mathbf{r}) \chi_c^{(-)*}(\mathbf{k}_c, \mathbf{r}_c) V_{bc}(\mathbf{r}_1) \\ & \times u_\ell(r_1) Y_m^\ell(\hat{r}_1) \chi_a^{(+)}(\mathbf{k}_a, \mathbf{r}_i), \end{aligned} \quad (2)$$

with $\hat{\ell} \equiv \sqrt{2\ell + 1}$. In Eq. (2), functions χ_i represent the distorted waves for the relative motions of various particles in their respective channels with appropriate boundary conditions. The superscripts (+) and (-) represents outgoing and ingoing wave boundary conditions, respectively. Arguments of these functions contain the corresponding Jacobi momenta and

coordinates. $V_{bc}(\mathbf{r}_1)$ represents the interaction between b and c , and $u_\ell(r_1)$ is the radial part of the corresponding wavefunction in the ground state of a . The position vectors satisfy the relations (see also Fig. 1 of Ref. [9]):

$$\mathbf{r} = \mathbf{r}_i - \alpha\mathbf{r}_1, \quad \alpha = \frac{m_c}{m_c + m_b}, \quad (3)$$

$$\mathbf{r}_c = \gamma\mathbf{r}_1 + \delta\mathbf{r}_i, \quad \delta = \frac{m_t}{m_b + m_t}, \quad \gamma = (1 - \alpha\delta), \quad (4)$$

where m_i ($i = a, b, c, t$) are the masses of various particles.

The reduced amplitude $\beta_{\ell m}$ [Eq. (2)] involves a six-dimensional integral which makes its evaluation quite complicated. The problem gets further aggravated due to the fact that the integrand involves the product of three scattering waves that exhibit an oscillatory behavior asymptotically. In order to facilitate an easier computation of Eq. (2), we perform a Taylor series expansion of the distorted waves of particles b and c about \mathbf{r}_i and write

$$\chi_b^{(-)}(\mathbf{k}_b, \mathbf{r}) = e^{-i\alpha\mathbf{K}_b \cdot \mathbf{r}_1} \chi_b^{(-)}(\mathbf{k}_b, \mathbf{r}_i), \quad (5)$$

$$\chi_c^{(-)}(\mathbf{k}_c, \mathbf{r}_c) = e^{i\gamma\mathbf{K}_c \cdot \mathbf{r}_1} \chi_c^{(-)}(\mathbf{k}_c, \delta\mathbf{r}_i). \quad (6)$$

Employing the LMA [28, 29], the magnitudes of momenta \mathbf{K}_j are taken as

$$K_j(R) = \sqrt{(2m_j/\hbar^2)[E_j - V_j(R)]}, \quad (7)$$

where m_j ($j = b, c$) is the reduced mass of the $j - t$ system, E_j is the energy of particle j relative to the target in the center of mass (c.m.) system, and $V_j(R)$ is the potential between j and t at a distance R . Substituting Eqs. (5) and (6) in Eq. (2), the amplitude $\beta_{\ell m_\ell}$ factorizes into two terms, each involving a three-dimensional integral,

$$\hat{\ell}\beta_{\ell m_\ell} = I_f \times I, \quad (8)$$

where

$$I_f = \int d\mathbf{r}_1 e^{-i\mathbf{Q} \cdot \mathbf{r}_1} V_{bc}(\mathbf{r}_1) u_\ell(r_1) Y_{m_\ell}^l(\mathbf{r}_1), \quad (9)$$

with

$$\mathbf{Q} = \gamma\mathbf{K}_c - \alpha\mathbf{K}_b, \quad (10)$$

and

$$I = \int d\mathbf{r}_i \chi_b^{(+)}(-\mathbf{k}_b, \mathbf{r}_i) \chi_c^{(+)}(-\mathbf{k}_c, \delta\mathbf{r}_i) \chi_a^{(+)}(\mathbf{k}_a, \mathbf{r}_i), \quad (11)$$

where we have used the relation $\chi^{(-)*}(\mathbf{k}, \mathbf{r}) = \chi^{(+)}(-\mathbf{k}, \mathbf{r})$.

Let us consider first the integral I . We expand the distorted wave for projectile-target relative motion in partial waves as

$$\chi_a^{(+)}(\mathbf{k}_a, \mathbf{r}_i) = \frac{4\pi}{k_a r_i} \sum_{L_a M_a} i^{L_a} f_{L_a}(k_a, r_i) Y_{M_a}^{L_a*}(\hat{\mathbf{k}}_a) Y_{M_a}^{L_a}(\hat{\mathbf{r}}_i), \quad (12)$$

where $f_{L_a}(k_a, r_i)$ is the radial part, calculated by solving the Schrödinger equation with proper optical potentials, which includes both Coulomb and nuclear terms. Beyond the range of the nuclear potential $f_{L_a}(k_a, r_i)$ has the form

$$f_{L_a}(k_a, r_i) \stackrel{r_i \rightarrow \infty}{\approx} \frac{i}{2} e^{i\sigma_{L_a}} [H_{L_a}^{(-)}(k_a r_i) - \epsilon_{L_a} H_{L_a}^{(+)}(k_a r_i)], \quad (13)$$

where $H_L^{(\pm)} = G_L \pm iF_L$, with F_L and G_L being the regular and irregular Coulomb wavefunctions, respectively, and ϵ_L is the scattering phase shift of the L^{th} partial wave. In Eq. (13), $\sigma_L = \arg\Gamma(L + 1 + i\eta)$ is the Coulomb phase shift with Coulomb parameter η .

Similar expansions can be written for the distorted waves for the core fragment and the valence particle relative motions:

$$\chi_b^{(+)}(-\mathbf{k}_b, \mathbf{r}_i) = \frac{4\pi}{k_b r_i} \sum_{L_b M_b} i^{-L_b} f_{L_b}(k_b, r_i) Y_{M_b}^{L_b}(\hat{\mathbf{k}}_b) Y_{M_b}^{L_b*}(\hat{\mathbf{r}}_i) \quad (14)$$

$$\chi_c^{(+)}(-\mathbf{k}_c, \delta\mathbf{r}_i) = \frac{4\pi}{k_c \delta r_i} \sum_{L_c M_c} i^{-L_c} f_{L_c}(k_c, \delta r_i) Y_{M_c}^{L_c}(\hat{\mathbf{k}}_c) Y_{M_c}^{L_c*}(\hat{\mathbf{r}}_i) \quad (15)$$

If $\hat{\mathbf{k}}_a$ (the incident beam direction) is chosen along the \hat{z} -direction, then the spherical harmonic, $Y_{M_a}^{L_a*}(\hat{\mathbf{k}}_a)$, in Eq. (12) simplifies to

$$\begin{aligned} Y_{M_a}^{L_a*}(\theta = 0, \phi = 0) &= \frac{\hat{L}_a}{\sqrt{4\pi}} \delta_{M_a, 0} \\ \Rightarrow M_a = 0 &\Rightarrow M_b = -M_c = M \text{ (say)}. \end{aligned} \quad (16)$$

Thereafter, substituting Eqs. (12), (14) and (15) in Eq. (11), we obtain

$$\begin{aligned} I &= \frac{(4\pi)^2}{k_a k_b k_c \delta} \sum_{L_a L_b L_c M} (-)^M (i)^{L_a - L_b - L_c} \hat{L}_b \hat{L}_c Y_M^{L_b}(\hat{\mathbf{k}}_b) Y_M^{L_c*}(\hat{\mathbf{k}}_c) \\ &\times \langle L_b M L_c - M | L_a 0 \rangle \langle L_b 0 L_c 0 | L_a 0 \rangle \\ &\times \int_0^\infty \frac{dr_i}{r_i} f_{L_a}(k_a, r_i) f_{L_b}(k_b, r_i) f_{L_c}(k_c, \delta r_i). \end{aligned} \quad (17)$$

Let us now turn our attention to integral I_f [Eq. (9)], which contains the structure information. Expanding the exponential, in Eq. (9), in partial waves, I_f simplifies to

$$I_f = 4\pi i^{-\ell} Y_{m_\ell}^\ell(\hat{\mathbf{Q}}) \int_0^\infty r_1^2 dr_1 j_\ell(Qr_1) u_\ell(r_1) V_{bc}(r_1). \quad (18)$$

Substituting Eqs. (17) and (18) in Eq. (8), we get

$$\begin{aligned} \hat{\ell}\beta_{\ell m} &= \frac{(4\pi)^3}{k_a k_b k_c \delta} i^{-\ell} Y_{m_\ell}^\ell(\hat{\mathbf{Q}}) Z_\ell(Q) \sum_{L_a L_b L_c} (i)^{L_a - L_b - L_c} \hat{L}_b \hat{L}_c \\ &\times \mathcal{Y}_{L_c}^{L_b}(\hat{k}_b, \hat{k}_c) \langle L_b 0 L_c 0 | L_a 0 \rangle \mathcal{R}_{L_b, L_c, L_a}(k_a, k_b, k_a), \end{aligned} \quad (19)$$

where

$$\mathcal{Y}_{L_c}^{L_b}(\hat{k}_b, \hat{k}_c) = \sum_M (-)^M \langle L_b M L_c - M | L_a 0 \rangle Y_M^{L_b}(\hat{k}_b) Y_M^{L_c*}(\hat{k}_c), \quad (20)$$

$$Z_\ell(Q) = \int_0^\infty r_1^2 dr_1 j_\ell(Qr_1) u_\ell(r_1) V_{bc}(r_1), \quad (21)$$

$$\mathcal{R}_{L_b, L_c, L_a} = \int_0^\infty \frac{dr_i}{r_i} f_{L_a}(k_a, r_i) f_{L_b}(k_b, r_i) f_{L_c}(k_c, \delta r_i). \quad (22)$$

The slowly converging radial integral $\mathcal{R}_{L_b, L_c, L_a}$ [Eq. (22)] can be effectively handled by using the complex plane method [27, 34]. $Y_{m_\ell}^\ell(\hat{\mathbf{Q}})$, in Eq. (19), whose argument contains the direction of a vector which is the sum of two other vectors [Eq. (10)], can be expressed in terms of spherical harmonics corresponding to directions of those vectors as [35]

$$\begin{aligned} (|\mathbf{Q}|)^\ell Y_{m_\ell}^\ell(\hat{\mathbf{Q}}) &= \sum_{LM_L} \frac{\sqrt{4\pi}}{\hat{\ell}} \binom{2\ell+1}{2L}^{1/2} (|\alpha K_b|)^{\ell-L} (\gamma K_c)^L \\ &\times \langle \ell - L m_\ell - M_L L M_L | \ell m_\ell \rangle \\ &\times Y_{m_\ell - M_L}^{\ell-L}(\hat{\mathbf{K}}_b) Y_{M_L}^L(\hat{\mathbf{K}}_c), \end{aligned} \quad (23)$$

where L runs from 0 to ℓ and

$$\binom{x}{y} = \frac{x!}{y!(x-y)!} \quad (24)$$

is the binomial coefficient.

This theory can be used to calculate breakup of both neutron and proton halo nuclei. Generally, the maximum value of the partial waves L_a, L_b, L_c must be very large in order to ensure the convergence of the partial wave summations in Eq. (19). However, for the case of

one-neutron halo nuclei, one can make use of the following method to include summations over infinite number of partial waves. We write $\beta_{\ell m}$ as

$$\beta_{\ell m} = \sum_{L_i=0}^{L_i^{max}} \hat{\beta}_{\ell m}(L_i) + \sum_{L_i=L_i^{max}}^{\infty} \hat{\beta}_{\ell m}(L_i), \quad (25)$$

where $\hat{\beta}$ is defined in the same way as Eq. (19) except for the summation sign and L_i corresponds to L_a , L_b , and L_c . If the value of L_i^{max} is chosen to be appropriately large, the contribution of the nuclear field to the second term of Eq. (25) can be neglected and we can write

$$\sum_{L_i=L_i^{max}}^{\infty} \hat{\beta}_{\ell m}(L_i) \approx \sum_{L_i=0}^{\infty} \hat{\beta}_{\ell m}^{Coul}(L_i) - \sum_{L_i=0}^{L_i^{max}} \hat{\beta}_{\ell m}^{Coul}(L_i), \quad (26)$$

where the first term on the right hand side, is the pure Coulomb breakup amplitude which for the case where one of the outgoing fragments is uncharged, can be expressed analytically in terms of the bremsstrahlung integral (see Ref. [9]). Therefore, only two terms, with reasonable upper limits, are required to be evaluated by the partial wave expansion in Eq. (25).

III. CALCULATIONS ON ^{11}Be

A. Structure model and optical potentials

The wavefunction, $u_{\ell}(r)$, appearing in the structure term, Z_{ℓ} , has been calculated by adopting a single particle potential model in the same way as in Ref. [9]. The ground state of ^{11}Be was considered to be a predominantly s -state with a $2s_{1/2}$ valence neutron coupled to the 0^+ ^{10}Be core [$^{10}\text{Be} \otimes 2s_{1/2}\nu$] with a one-neutron separation energy of 504 keV and a spectroscopic factor of 0.74 [36]. The single particle wavefunction was constructed by assuming the valence neutron- ^{10}Be interaction to be of Woods-Saxon type whose depth was adjusted to reproduce the corresponding value of the binding energy with fixed values of the radius and diffuseness parameters (taken to be 1.15 fm and 0.5 fm, respectively). This gave a potential depth of 71.03 MeV, a root mean square (rms) radius for the valence neutron of 6.7 fm, and a rms radius for ^{11}Be of 2.91 fm when the size of the ^{10}Be core was taken to be 2.28 fm. The neutron-target optical potentials used by us were extracted from the global set of Bechetti-Greenlees (see, e.g, [37]), while those used for the ^{10}Be -target ([37, 38])

system are shown in Table I. Following [31], we have used the sum of these two potentials for the ^{11}Be -target channel. We found that values of L_i^{max} of 500 for Au, Ta, U, Pb and Ti targets and 150 for Be and C targets provided very good convergence of the corresponding partial wave expansion series [Eq. (19)]. The local momentum wave vectors are evaluated at a distance, $R = 10$ fm in all the cases, and their directions are taken to be same as that of asymptotic momenta (see appendix A).

TABLE I: Optical potential parameters for the ^{10}Be -target interaction. Radii are calculated with the $r_j t^{1/3}$ convention.

system	V_r (MeV)	r_r (fm)	a_r (fm)	W_i (MeV)	r_i (fm)	a_i (fm)
$^{10}\text{Be}-^{197}\text{Au}$	400	2.08	0.9	76.2	1.52	0.38
$^{10}\text{Be}-^{208}\text{Pb}$	400	2.08	0.9	76.2	1.52	0.38
$^{10}\text{Be}-^{44}\text{Ti}$	70	2.5	0.5	10.0	1.5	0.50
$^{10}\text{Be}-^9\text{Be}$	100	2.6	0.5	18.0	2.6	0.50

B. Neutron energy distribution

In Fig. 1, we present the results of our calculations for the double differential cross section as a function of neutron energy for two neutron angles (1° and 3.4°), in the breakup of ^{11}Be on Au at the beam energy of 41 MeV/nucleon. The core scattering angle in the laboratory system has been integrated from 0° to 30° . The dotted and dashed lines represent the pure Coulomb and pure nuclear contributions, respectively, while their coherent and incoherent sums are shown by the solid and dot-dashed lines, respectively. The plus signs and the inverted solid triangles represent the magnitudes of the positive and negative interference terms, respectively.

The CNI terms are seen to be dependent on angles and energies of the outgoing neutron. Their magnitudes are nearly equal to those of the nuclear breakup contributions which leads to a difference in the incoherent and coherent sums of the Coulomb and nuclear contributions underlying thus the importance of these terms.

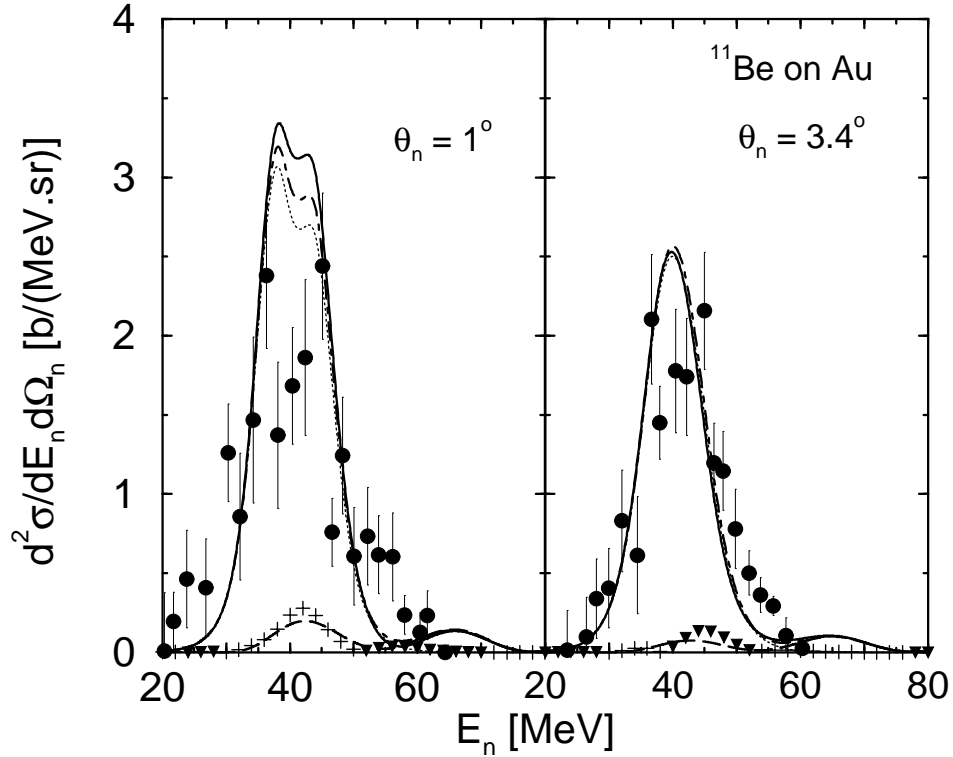


FIG. 1: Neutron energy distribution for the breakup reaction ^{11}Be on Au at the beam energy of 41 MeV/nucleon, at the neutron angles of 1° and 3.4° . The dotted and dashed lines represent the pure Coulomb and nuclear contributions, respectively while their coherent and incoherent sums are shown by the solid and dot-dashed lines, respectively. The plus signs and the inverted solid triangles represent the magnitudes of the positive and negative interference terms, respectively. The data are taken from [21].

C. Relative energy spectra

The relative energy spectrum of the fragments (neutron and ^{10}Be) emitted in the breakup of ^{11}Be on ^{208}Pb (top panel), ^{44}Ti (middle panel) and ^{12}C (bottom panel) targets at the beam energy of 72 MeV/nucleon is shown in Fig. 2. In these calculations the integration over the projectile c.m. angle ($\theta_{n^{10}\text{Be-Pb}}$) has been done in the range of 0° – 40° , mainly to include the effects of nuclear breakup coming from small impact parameters. The relative angle between the fragments ($\theta_{n-^{10}\text{Be}}$) has been integrated from 0° to 180° . The dotted and dashed lines represent the pure Coulomb and nuclear breakup contributions, respectively while their

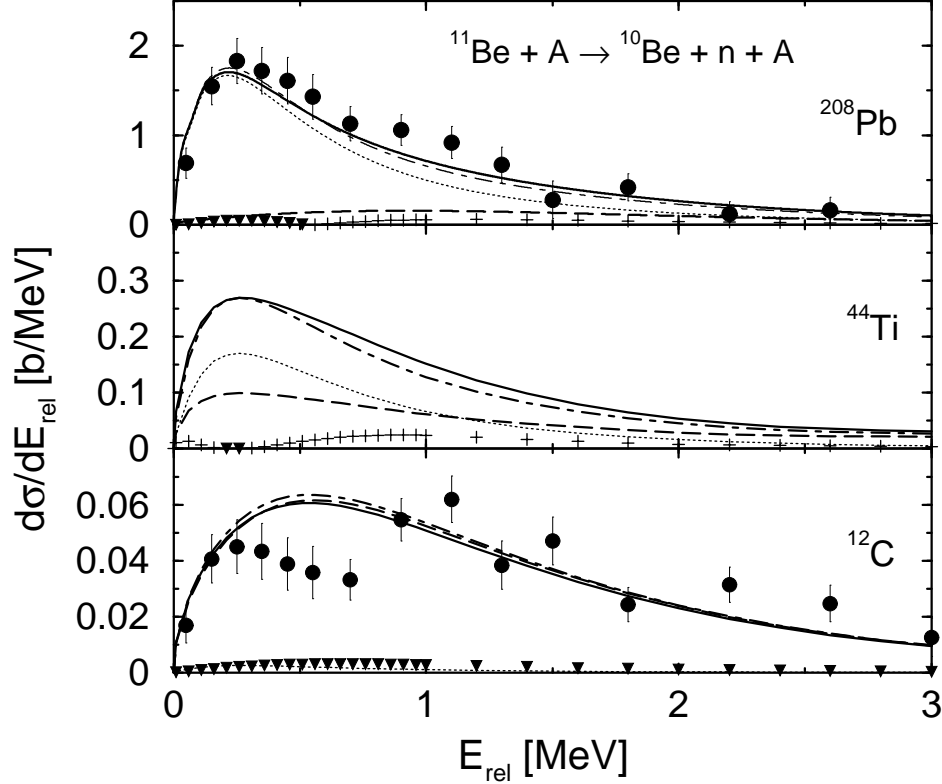


FIG. 2: The differential cross section as a function of the relative energy of the fragments (neutron and ^{10}Be) in the breakup reaction of ^{11}Be on ^{208}Pb , ^{44}Ti and ^{12}C targets at 72 MeV/nucleon. The dotted and dashed lines represent the pure Coulomb and nuclear breakup contributions, respectively while their coherent and incoherent sums are shown by the solid and dot-dashed lines, respectively. The plus signs and the inverted triangles represent the magnitudes of the positive and negative interference terms, respectively. The data are taken from [5].

coherent and incoherent sums are shown by the solid and dot-dashed lines, respectively. The plus signs and the inverted triangles represent the magnitudes of the positive and negative interference terms, respectively.

In case of breakup on a heavy target (^{208}Pb) [Fig. 2 (top panel)] the pure Coulomb contributions dominate the cross sections around the peak value, while at larger relative energies the nuclear breakup is important. This is attributed to the different energy dependence of the two contributions [31]. The nuclear breakup occurs when the projectile and the target nuclei are close to each other. Its magnitude, which is determined mostly by the geometrical conditions, has a weak dependence on the relative energy of the outgoing fragments beyond

a certain minimum value. In contrast, the Coulomb breakup contribution has a long range and it shows a strong energy dependence. The number of virtual photons increases for small excitation energies and hence the cross sections rise sharply at low excitation energies. After a certain value of this energy the cross sections decrease due to setting in of the adiabatic cut-off. The coherent sum of the Coulomb and nuclear contributions provides a good overall description of the experimental data. The nuclear and the CNI terms are necessary to explain the data at larger relative energies.

In the middle panel of Fig. 2, we show the relative energy of the fragments in the breakup of ^{11}Be on a medium mass target (^{44}Ti). At low relative energies the pure Coulomb contributions are slightly higher than the pure nuclear ones, while at higher relative energies it is the nuclear part which dominates. Apart from the very low relative energy region the CNI terms play an important role, which is clearly borne out by the difference in the coherent (solid) and incoherent (dot-dashed) sums of the pure Coulomb and pure nuclear contributions.

The relative energy spectra for the breakup on a light target (^{12}C) is shown in the bottom panel of Fig. 2. In this case we have used the same optical potential for the ^{10}Be - ^{12}C system as in the ^{10}Be - ^9Be case, which we had used earlier in calculating the neutron angular distribution in Ref. [26]. The total cross section in this case is normalized to the experimental cross section (found by integrating the area under the data points) and the same normalization constant is used for all the cross sections in this case. The breakup is clearly seen to be nuclear dominated at all relative energies, and the pure Coulomb and CNI terms have very little contributions.

The importance of the peripheral region even in nuclear dominated reactions is underlined in Fig. 3. In this figure, we show a comparison of the angular distribution of the single neutron observed in the elastic breakup of ^{11}Be on a ^9Be target at the beam energy of 41 MeV/nucleon, calculated with (dashed line) and without (solid line) a lower cut-off of 10 fm in the r_i integral [Eq. (22)]. The close similarity of the two results shows the importance of the peripheral region in this reaction. This fact is further strengthened by noting that the total one-neutron removal cross sections calculated with and without cut-off are found to be 0.128 b and 0.189 b, respectively. Thus, almost 70% of this cross section is accounted for by regions larger than 10 fm. This is a consequence of the large spatial extent of ^{11}Be , which allows it to interact with the target nucleus even at a larger distance.

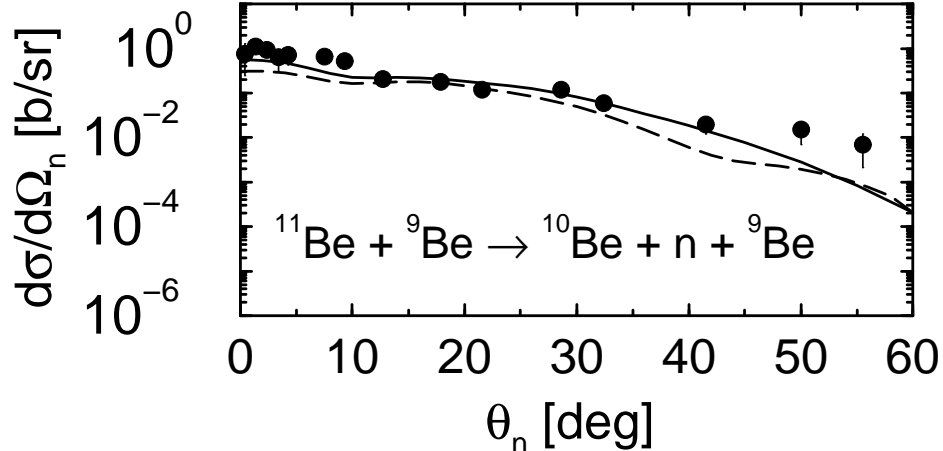


FIG. 3: The neutron angular distribution in the breakup of ^{11}Be on Be at 41 MeV/nucleon. The dashed line shows the calculation where a lower cut-off of 10 fm is applied in the r_i integral [Eq. (22)] while the solid line shows the result without any cut-off. The data are taken from [21].

D. Parallel momentum distribution

The parallel momentum distributions (PMDs) of the ^{10}Be fragment in the breakup of ^{11}Be on U and Ta targets, at 63 MeV/nucleon beam energy are presented in the rest frame of the projectile, in Fig. 4. The core transverse momentum has been integrated from 0-500 MeV/c and the neutron angle (θ_n) has been integrated from 0° to 30° . We have used the following sets of optical potentials here: $V_r = 200$ MeV, $r_r = 1.23$ fm, $a_r = 0.9$ fm, $W_i = 76.2$ MeV, $r_i = 1.49$ fm, $a_i = 0.38$ fm for the U target and $V_r = 200$ MeV, $r_r = 1.26$ fm, $a_r = 0.9$ fm, $W_i = 76.2$ MeV, $r_i = 1.53$ fm, $a_i = 0.38$ fm for the Ta target. The dotted and dashed lines show the contributions of the pure Coulomb and nuclear breakups, respectively, while their coherent sums are represented by solid lines. The coherent sum is normalized to the peak of the data, which are given in arbitrary units, and the same normalization factor has been used for the pure Coulomb and pure nuclear contributions.

It is seen that around the peak region, the Coulomb contributions dominate. This is because most of the contributions in this region come from forward angles, where Coulomb breakup is the predominant mode. However, in the wings of the distribution (beyond about $|p_z| = 40$ MeV/c), contributions come from large scattering angles and consequently the pure nuclear breakup dominates, in this region.

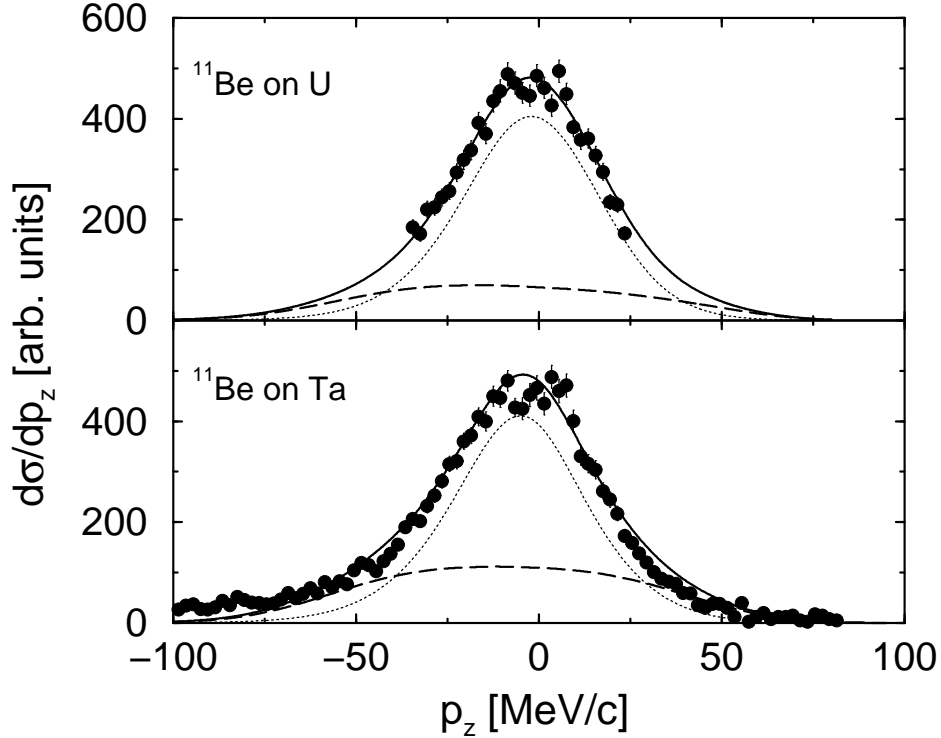


FIG. 4: The parallel momentum distribution of the core in the breakup of ^{11}Be on U and Ta targets, at 63 MeV/nucleon beam energy, in the rest frame of the projectile. The dotted and dashed lines represent the pure Coulomb and nuclear breakup contributions, respectively while their coherent sums are shown by solid lines. The data are taken from [39].

The FWHM of the distributions on U and Ta targets are found to be 48 MeV/c and 49 MeV/c, respectively. The width of the fragment momentum distribution can be qualitatively related to the radial extent of the coordinate space nuclear wavefunction of the projectile via Heisenberg's uncertainty principle. Thus a narrow PMD width implies a large spatial extension of the nuclear wavefunction in the coordinate space for ^{11}Be .

Our calculations with medium mass ^{44}Ti and light ^9Be targets also leads us to similar conclusions. In Fig. 5 we present the PMDs of the ^{10}Be fragment in the breakup of ^{11}Be on ^{44}Ti and ^9Be targets, at 63 MeV/nucleon beam energy, in the rest frame of the projectile. The integrations over the transverse momentum and the neutron angle have been performed over the same range as in the case of heavy targets. The dotted and the dashed lines are the pure Coulomb and pure nuclear contributions, respectively, while their coherent sums are represented by solid lines. In case of breakup on a medium mass target (^{44}Ti) [Fig. 5 (lower

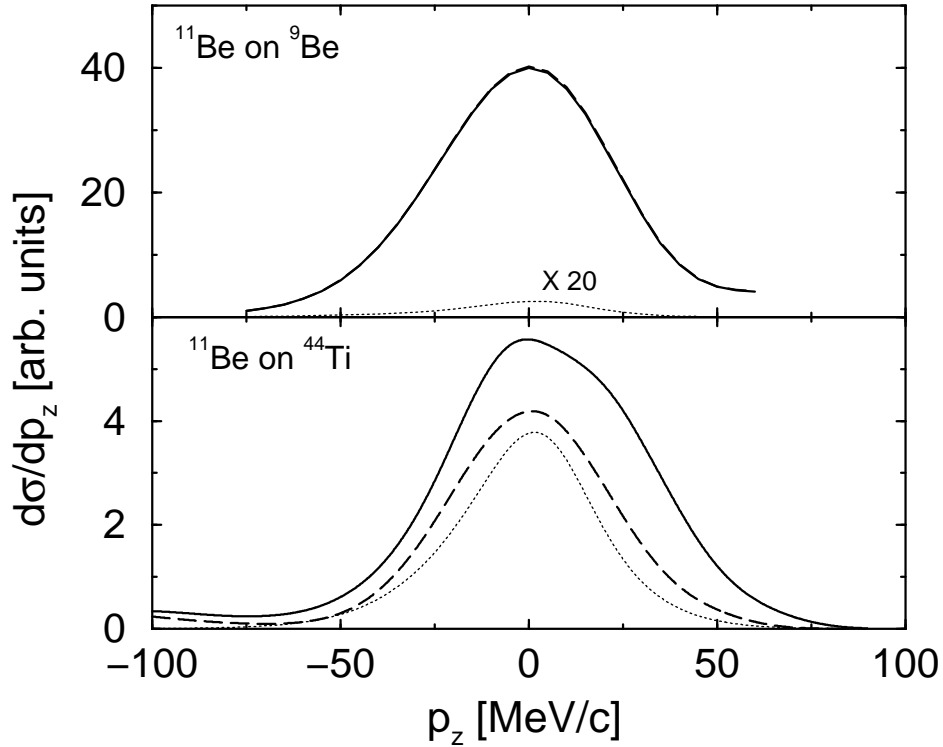


FIG. 5: The parallel momentum distribution of the core in the breakup of ^{11}Be on ^9Be and ^{44}Ti targets, at 63 MeV/nucleon beam energy, in the rest frame of the projectile. The dotted and dashed lines represent the pure Coulomb and nuclear breakup contributions, respectively while their coherent sums are shown by solid lines. The pure Coulomb contribution in case of breakup on a ^9Be target is multiplied by a factor of 20 to make it visible.

panel)] the pure Coulomb and pure nuclear contributions have nearly equal contributions, as has been seen while calculating the relative energy spectra of the fragments. Breakup on a light target (^9Be) [Fig. 5 (upper panel)] is expectedly pure nuclear dominated. The pure Coulomb contribution is extremely small and is in fact multiplied by 20 to make it visible. The pure nuclear (dashed line) and the coherent sum (solid line) of the pure nuclear and pure Coulomb contributions thus almost coincide with each other. The FWHM of the distributions on ^{44}Ti and ^9Be targets are found to be 60 MeV/c and 56 MeV/c, respectively. They are in line with the low widths mentioned earlier with heavy targets.

TABLE II: Total one-neutron removal cross section, various contributions from pure Coulomb and pure nuclear breakups, and their incoherent sum for ^{11}Be breakup on Au, Ti and Be targets, at beam energy of 41 MeV/nucleon.

Target	Total	Pure Coulomb	Pure nuclear	Incoherent sum	Expt. [21]
	(b)	(b)	(b)	(b)	(b)
^{197}Au	2.10	1.88	0.21	2.09	2.5 ± 0.5
^{44}Ti	0.403	0.177	0.189	0.37	0.55 ± 0.11
^9Be	0.189	0.006	0.181	0.187	0.24 ± 0.05

E. Total one-neutron removal cross section

In Table II, we show the contributions of pure Coulomb and pure nuclear breakup mechanisms to the total one-neutron removal cross sections in the breakup of ^{11}Be on Au, Ti and Be targets at the beam energy of 41 MeV/nucleon. The incoherent sum is obtained by simply adding the pure Coulomb and pure nuclear cross sections.

For the heavy mass, high-Z target (Au) case it is seen that pure Coulomb breakup accounts for about 90% of the total cross section. On a medium mass, medium-Z target (Ti), the pure Coulomb and nuclear contributions to the total cross section, are nearly equal to each other, while for the low mass, low-Z target (Be), the pure nuclear contribution accounts for almost all of the total cross section.

The total one-neutron removal cross section on Au and Be targets does not seem to be affected by the CNI terms, while for the Ti target case the incoherent sum seems to be about 10% less than the total cross section. Thus, it seems that the CNI terms manifests themselves more explicitly in more exclusive measurements, like double differential cross sections than in quantities like total cross sections.

IV. SUMMARY AND CONCLUSIONS

In this paper we have presented an extended version of a fully quantum mechanical theory of halo breakup reactions [26] within the framework of post-form DWBA, where the pure Coulomb, pure nuclear as well as their interference terms are treated consistently within

the same framework. In this theory, both the Coulomb and nuclear interactions between the projectile and the target nucleus are treated to all orders, but the fragment-fragment interaction is treated in the first order. The full ground state wavefunction of the projectile corresponding to any orbital angular momentum structure enters as an input to this theory. The lack of proper knowledge of appropriate optical potentials, particularly in the halo projectile-target channel is a source of uncertainty in the calculations. However this is the case for all reaction studies of halo nuclei where distorted waves in the projectile-target channel are used, as has already been pointed out in Ref. [26].

We applied our theory to study the breakup of one-neutron halo nucleus ^{11}Be on several targets. Results for the neutron energy distribution in the breakup of ^{11}Be on Au at 41 MeV/nucleon emphasize the fact that the Coulomb-nuclear interference terms are both energy and angle dependent. They are almost of the same magnitude as the nuclear breakup contributions and this leads to a difference in the coherent and incoherent sums of the Coulomb and nuclear terms, more so at forward angles. The parallel momentum distribution of the ^{10}Be fragment in the breakup reaction of ^{11}Be in the Coulomb and nuclear fields of U and Ta targets have also been calculated at 63 MeV/nucleon. It is seen that the region around the peak of the distribution, which gets substantial contributions from forward scattered fragments, is Coulomb dominated, while in the wings of the distribution, where contributions come from fragments scattered at large angles, the nuclear breakup contributions dominate. The FWHMs of the distributions were also found to be small consistent with the expectation of the wavefunction of ^{11}Be to have a large spatial extent in the coordinate space. Parallel momentum distributions in the breakup on medium mass (Ti) and light (Be) targets also confirmed a small FWHM. The relative energy spectra of the fragments (neutron and ^{10}Be) emitted in the breakup of ^{11}Be on Pb, Ti and C targets, at the beam energy of 72 MeV/nucleon have also been calculated. While the breakup on the light target was highly nuclear dominated, that on a heavy target required the nuclear and the CNI terms for a better explanation of the data particularly at higher relative energies. In case of breakup on a medium mass target, the total pure Coulomb and pure nuclear contributions were nearly equal in magnitude. The CNI terms were found to have little impact on the total one-neutron removal cross section in the breakup of ^{11}Be on heavy and light targets at the beam energy of 41 MeV/nucleon, but on a medium mass (Ti) target the CNI terms were almost 10% of the total one-neutron removal cross section. Thus in many

sophisticated experiments planned in the future one has to look into the role played by the CNI terms in analyzing the experimental data.

The full quantal theory of one-neutron halo breakup reactions, presented in this paper, can be applied to describe the $(a, b\gamma)$ reaction provided the inelastic breakup mode is also calculated within this theory. These studies are in progress. There is also a need to extend the theory to describe the halo breakup at higher beam energies for which data have been taken at GSI, Darmstadt. This can be achieved by introducing the eikonal expansion of the distorted waves, instead of the partial wave expansion as done here.

Acknowledgments

It is a pleasure to thank Prof. R. Shyam for many illuminating discussions and for going through the manuscript. Thanks, also to Prof. T. Nakamura for providing the experimental data shown in the bottom panel of Fig. 2 in a tabular format.

APPENDIX A: VALIDITY OF THE LOCAL MOMENTUM APPROXIMATION

The LMA provides a way of taking into account the finite range effects in the DWBA theory. It leads to the factorization of the breakup amplitude [Eq. (2)], which makes its numerical calculation relatively simpler. As discussed in Ref. [28], a condition of validity of the LMA is that the quantity

$$\eta(r) = \frac{1}{2}K(r)|dK(r)/dr|^{-1} \quad (\text{A1})$$

evaluated at a representative distance R should be larger than the projectile radius (r_a). In our case the LMA is done on both the outgoing fragments (b and c). In Fig. 6, we show the variation of $\eta_b(r)$ (top half) and $\eta_c(r)$ (bottom half) with r , for the breakup of ^{11}Be on a Pb target, at the beam energy of 72 MeV/nucleon (left half) and ^{11}Be on a Be target at the beam energy of 41 MeV/nucleon (right half), where both Coulomb and nuclear potentials are included in the term $V_j(r)$ in the definition of $K(r)$ [Eq. (7)]. At $r = 10$ fm, $\eta_b(r) = 185$ fm and $\eta_c(r) = 108$ fm for ^{11}Be incident on a Pb target and $\eta_b(r) = 914$ fm and $\eta_c(r) = 3892$ fm for ^{11}Be incident on a Be target. These values are much larger than the rms radius of ^{11}Be , which is about 2.91 fm. (Incidentally, the spikes and turns in $\eta(r)$ at low r are due to the presence of the short ranged nuclear potential.)

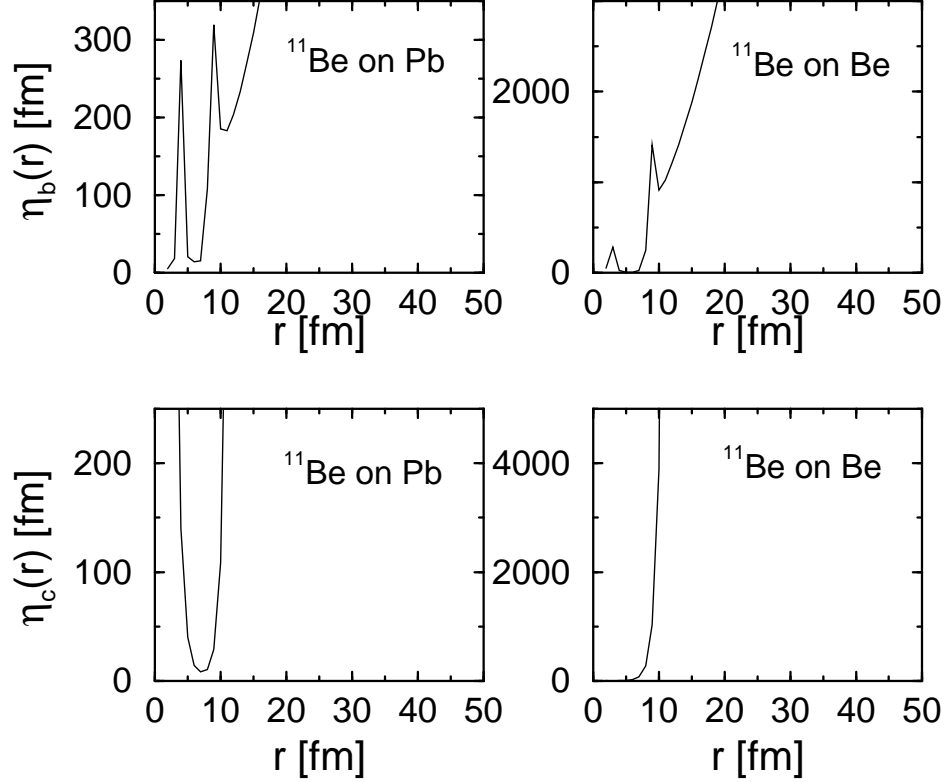


FIG. 6: Variation of $\eta_b(r)$ (top half) and $\eta_c(r)$ (bottom half) with r , for the breakup of ^{11}Be on Pb, at 72 MeV/nucleon (left half) and ^{11}Be on Be at 41 MeV/nucleon (right half).

The variations of $K_b(r)$ and $K_c(r)$, the magnitudes of the local momentum (LM), with r for the above mentioned reactions are shown in Fig. 7. We see that $K_b(r)$ and $K_c(r)$ remains practically constant for $r > 8$ fm. Due to the peripheral nature of breakup reactions, this region contributes maximum to the cross section. Therefore, our choice of a constant magnitude for the local momentum evaluated at 10 fm is well justified. Thus the condition of validity of the LMA is well fulfilled in these cases.

We have also performed calculations for different LM directions of b and c . We denote the different combination of directions as D_1 : both the LM angles of b and c are taken along asymptotic directions, D_2 : the LM angles of b are taken to be zero while the LM angles of c are taken along the asymptotic direction, D_3 : the LM angles of b are taken to be half those of the asymptotic direction while the LM angles of c are taken along the asymptotic direction, D_4 : the LM angles of b are taken along the asymptotic direction while the LM angles of c are taken to be zero, D_5 : the LM angles of b are taken along the asymptotic

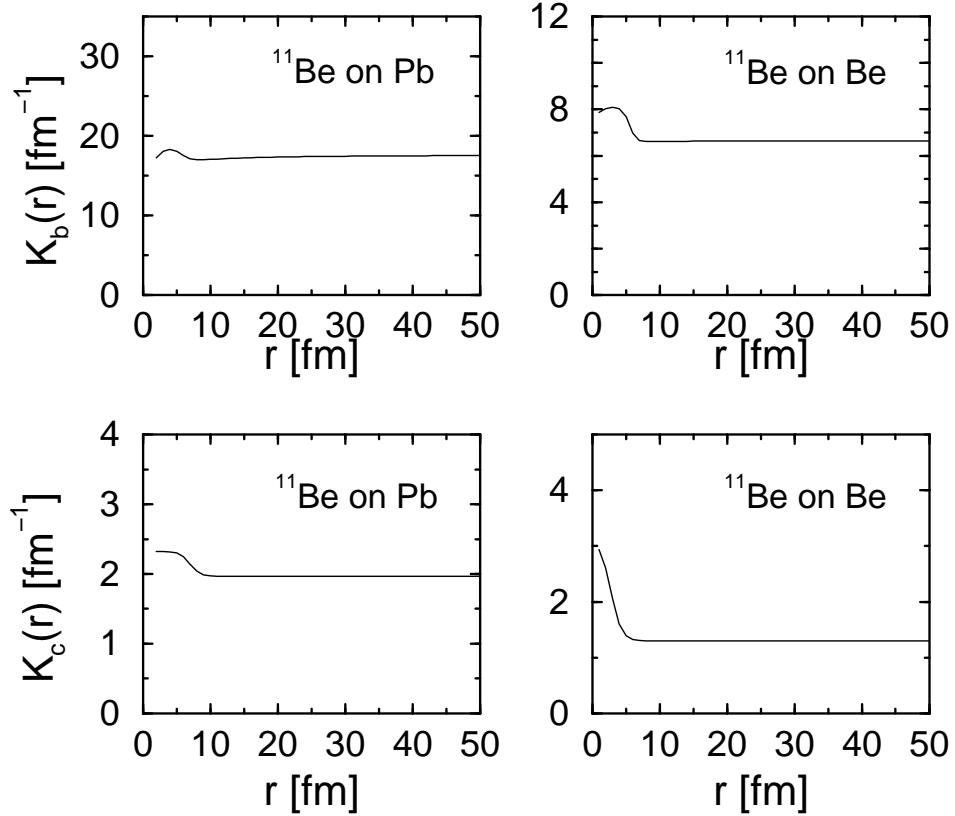


FIG. 7: Variation of $K_b(r)$ (top half) and $K_c(r)$ (bottom half) with r , for the breakup of ¹¹Be on Pb, at 72 MeV/nucleon (left half) and ¹¹Be on Be at 41 MeV/nucleon (right half).

direction while the LM angles of c are taken to be half those of the asymptotic direction, D_6 : both the LM angles of b and c are taken to be zero, and D_7 : both the LM angles of b and c are taken to be half those of asymptotic directions. In Table III, we present the

TABLE III: Calculated value of the total one-neutron removal cross section for ¹¹Be on Au and Be targets at 41 MeV/nucleon for different local momentum directions (see text).

Projectile	D_1	D_2	D_3	D_4	D_5	D_6	D_7
+ target	(b)						
¹¹ Be + Au	2.10	2.13	2.14	2.16	2.10	2.24	2.29
¹¹ Be + Be	0.189	0.204	0.192	0.167	0.162	0.141	0.150

total one-neutron removal cross section in the breakup of ¹¹Be on Au and Be targets at 41

MeV/nucleon for different directions of the LM. We note that these cross sections depend on the local momentum directions only to the extent of 10 – 15%.

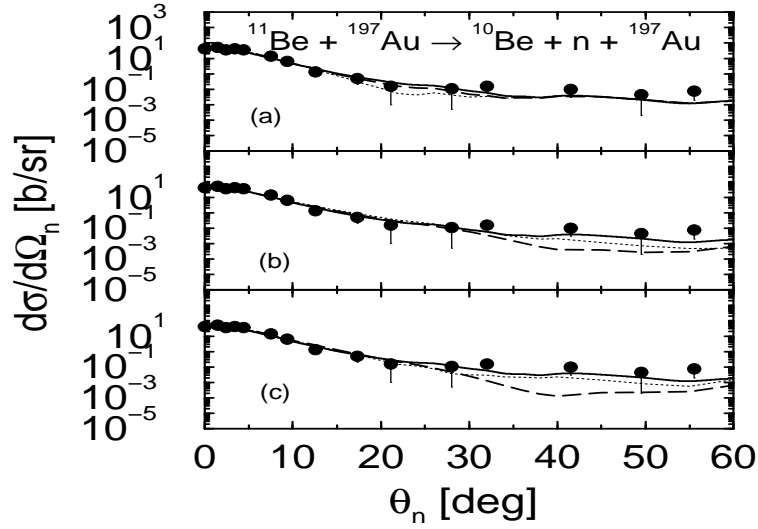


FIG. 8: The neutron angular distribution for the breakup reaction $^{11}\text{Be} + \text{Au} \rightarrow ^{10}\text{Be} + n + \text{Au}$, at 41 MeV/nucleon for different LM directions (see text).

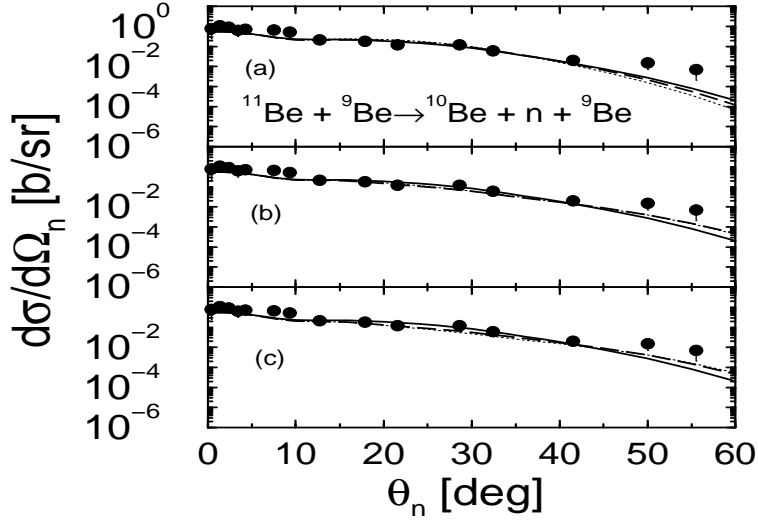


FIG. 9: The neutron angular distribution for the breakup reaction $^{11}\text{Be} + \text{Be} \rightarrow ^{10}\text{Be} + n + \text{Be}$, at 41 MeV/nucleon for different LM directions (see text).

In Figs. 8 and 9, we show the variation of the neutron angular distribution for different combinations of LM directions of the core and the valence neutron in the breakup of ^{11}Be

on Au and Be targets, respectively, at 41 MeV/nucleon. In both the figures, the solid line shows the calculation with direction D_1 . In panel (a), of both Figs. 8 and 9, calculations are shown for directions D_2 (dotted line) and D_3 (dashed line), panel (b) shows it for D_4 (dotted line) and D_5 (dashed line), while panel (c) shows the same for D_6 (dotted line) and D_7 (dashed line). We see that for the Be target case the neutron angular distributions are minimally dependent on various LM directions, but for the Au target case, some dependence is observed at large angles. However, the magnitudes of the cross sections here are very small. Consequently no such angular dependence will be observed in cross sections which involve angular integrations for both the outgoing fragments or in more inclusive cross sections.

-
- [1] P.G. Hansen and B.M. Sherill, Nucl. Phys. A **693**, 133 (2001).
 - [2] I. Tanihata, Nucl. Phys. A **654**, 235c (1999); J. Phys. G **22**, 157 (1996).
 - [3] K. Riisager, Rev. Mod. Phys. **66**, 1105 (1994).
 - [4] C.A. Bertulani, L.F. Canto and M.S. Hussain, Phys. Rep. **226**, 281 (1993).
 - [5] T. Nakamura *et al.*, Phys. Lett. B **331**, 296 (1994).
 - [6] T. Nakamura *et al.*, Phys. Rev. Lett **83**, 1112 (1999).
 - [7] P. Banerjee, I.J. Thompson and J.A. Tostevin, Phys. Rev. C **58**, 1042 (1998).
 - [8] P. Banerjee, I.J. Thompson and J.A. Tostevin, Phys. Rev. C **58**, 1337 (1998).
 - [9] R. Chatterjee, P. Banerjee and R. Shyam, Nucl. Phys. A **675**, 477 (2000).
 - [10] R. Chatterjee, P. Banerjee and R. Shyam, Nucl. Phys. A **692**, 476 (2001).
 - [11] R. Chatterjee and P. Banerjee, Phys. Rev. C **63**, 017303 (2001).
 - [12] G.F. Bertsch, K. Hencken, and H. Esbensen, Phys. Rev. C **57**, 1366 (1998); H. Esbensen and G.F. Bertsch, Phys. Rev. C **59**, 3240 (1999).
 - [13] A. Bonaccorso and F. Carstoiou, Phys. Rev. C **61**, 034605 (2000) and references therein.
 - [14] K. Yabana, Y. Ogawa and Y. Suzuki, Nucl. Phys. A **539**, 295 (1992).
 - [15] P.G. Hansen, A.S. Jensen and B. Jonson, Annu. Rev. Nucl. Part. Sci. **45**, 2 (1995).
 - [16] B. Davids *et al.*, Phys. Rev. Lett. **81**, 2209 (1998).
 - [17] D. Cortina-Gil *et al.*, Eur. Phys. J. A **10**, 49 (2001).
 - [18] R. Kanungo *et al.*, Phys. Rev. Lett. **88**, 142402 (2002).
 - [19] U. Datta Pramanik *et al.*, Phys. Lett. B **551**, 63 (2003).

- [20] R. Anne *et al.*, Phys. Lett. B **250**, 19 (1990).
- [21] R. Anne *et al.*, Nucl. Phys. A **575**, 125 (1994).
- [22] P. Banerjee and R. Shyam, Nucl. Phys. A **540**, 112 (1993); J. Phys. G **22**, L79 (1996).
- [23] V. Maddalena and R. Shyam, Phys. Rev. C **63**, 051601 (2001).
- [24] G. Baur, F. Rösler, D. Trautmann and R. Shyam, Phys. Rep. **111**, 333 (1984).
- [25] G.R. Satchler, Nucl. Phys. **55**, 1 (1964).
- [26] R. Chatterjee and R. Shyam, Phys. Rev. C **66** (2002) 061601(R).
- [27] R. Chatterjee, Ph.D. Thesis, Jadavpur University, Kolkata (2003), available from the author by sending an e-mail to *raja@theory.saha.ernet.in* .
- [28] R. Shyam and M.A. Nagarajan, Ann. Phys. (NY) **163**, 285 (1985).
- [29] P. Braun-Munzinger and H.L. Harney, Nucl. Phys. **A233**, 381 (1974).
- [30] R. Shyam and I.J. Thompson, Phys. Rev. C **59**, 2645 (1999).
- [31] S. Typel and R. Shyam, Phys. Rev. C **64**, 024605 (2001).
- [32] J. Margueron, A. Bonaccorso and D.M. Brink, Nucl. Phys. A **703**, 105 (2002).
- [33] J. Margueron, A. Bonaccorso and D.M. Brink, Nucl. Phys. A **720**, 337 (2003).
- [34] C.M. Vincent and H.T. Fortune, Phys. Rev. C **2**, 782 (1970).
- [35] M. Moshinski, Nucl. Phys. **13**, 104 (1959).
- [36] T. Aumann *et al.*, Phys. Rev. Lett. **84**, 35 (2000).
- [37] C.M. Perey and F.G. Perey, Atomic Data and Nuclear Data Tables **17**, 1 (1976).
- [38] M. Beunard *et al.*, Nucl. Phys. A **424**, 313 (1984).
- [39] J.H. Kelley *et al.*, Phys. Rev. Lett. **74**, 30 (1995).